Gas-phase synthesis of nanoparticles of group 12 chalcogenides

Nigel L. Pickett,[a] Frank. G. Riddell,[a] Douglas F. Foster,[a] David J. Cole-Hamilton*[a] and John R. Fryer[b]

[a]*School of Chemistry, The University of St. Andrews, St. Andrews, Fife, Scotland, UK, KY16 9ST*
[b]*Department of Chemistry, Glasgow University, Glasgow, Scotland, UK, G12 8QQ*

The effect of pyridine addition upon the gas-phase reactions of hydrogen sulfide (H_2S) or hydrogen selenide (H_2Se) with either dimethylcadmium (Me_2Cd) or dimethylzinc (Me_2Zn) has been investigated. The deposits of CdS, CdSe, ZnSe or ZnS which form have been analysed by powder X-ray diffraction (PXRD), elemental analysis and transmission electron microscopy (TEM). At ambient temperatures the deposits consist of particles in the nanocrystalline size range of the hexagonal phase. The average particle size within the deposits is dependent upon the concentration of pyridine in the gas phase, the temperature at which the reactants are mixed and, in the case of ZnSe, whether an inert (He) or reducing (H_2) carrier gas is used. At ambient temperatures in an inert carrier gas, the control of particle size exerted by pyridine decreases in the order ZnS > CdS > CdSe > ZnSe, although in hydrogen, the prereaction between Me_2Zn and H_2Se could be almost completely eliminated by raising the temperature. Further investigation of CdS deposits have been carried out by photoacoustic spectroscopy (PAS) to access the band-gap, and solid-state ^{13}C and ^{113}Cd NMR to probe the surface state of the particles. Elemental analysis and the NMR studies suggest that pyridine binds through the lone pair of the nitrogen to surface metal atoms on growing particles, inhibiting further particle growth. The particle size is greatly dependent upon the strength of the pyridine–surface metal atom interaction, the acidity of the EH bond (E = S or Se) and the polarity of the MMe bond (M = Zn or Cd). In hydrogen, it is proposed that amide species may form and be responsible for growth inhibition.

The use of metal organic vapour phase epitaxy (MOVPE) to produce single-crystal layers of wide band-gap 12–16 (II–VI) materials (ZnS, ZnSe, CdS and CdSe), is now a favoured technique. The most common method employs the thermally controlled reaction between a group 12 dialkyl compound, R_2M (R = Me, Et *etc.*; M = Zn and Cd) and a group 16 hydride (H_2S or H_2Se).[1–3] This technique has, however, been hampered by the premature reaction (prereaction) which occurs between the two gas-phase precursors in the cold zone of the growth cell, upstream of the heated substrate. Prereaction has an adverse effect on the materials grown, leading to layer thickness non-uniformity which in turn affects the optoelectronic properties of the grown materials. The origins of this prereaction have been attributed to the proficient elimination of the alkyl groups from the group 12 precursor in the presence of the acidic hydrogens of the group 16 hydride.

It has been shown that the introduction of a σ-donor compound to the reaction system, either in the form of an adduct with the group 12 alkyl precursor, which in turn can give added advantages in more convenient vapour pressures,[4] or by direct addition to the carrier gas flow, leads to a reduction of prereaction. Compounds which have been investigated as prereaction suppression reagents include the oxygen donor compound 1,4-dioxan,[5–7] the oxygen–sulfur compound thioxan,[7] along with a number of nitrogen σ-donor compounds[8,9] which include triethylamine,[10,11] 1,3,5-trimethylhexahydro-1,3,5-triazine,[11] *N,N,N′,N′*-tetramethylethane-1,2-diamine,[12] *N,N,N′,N′*-tetramethyldiaminomethane[13] and pyridine.[14]

Introduction of pyridine into the gas phase during MOVPE growth of ZnSe when using Me_2Zn and H_2Se, even at concentrations well below a stoichiometric equivalent, can virtually eliminate the prereaction, with no apparent deposit seen upstream and only a small amount of yellow deposit downstream of the heated substrate. The presence of pyridine also leads to marked improvements in both the growth rate and optoelectronic properties of ZnSe epilayers.[14] Similar addition of pyridine fails to inhibit prereaction between Me_2Cd and H_2Se, with the only noticeable change being in the colour of the solid deposit upstream of the substrate from black to red. Epilayers of CdSe grown in the presence of pyridine do, however, show greater uniformity and improved optoelectronic properties.[14] The introduction of pyridine into ZnS and CdS growth systems has yet to be reported.

The mechanism by which σ-donor compounds reduce prereaction during the growth of II/VI materials, and their role in improving growth rates and optoeletronic properties of the final epilayers, is poorly defined but of considerable debate. Several proposed mechanisms for the inhibition of prereaction have previously been reported.[8,14,15] The first suggests the prereaction occurs through an initial step involving the gas-phase formation of a weak adduct between the group 16 hydride and the metal dialkyl compound which, *via* the reductive elimination of saturated hydrocarbons, leads to the formation of a solid deposit of the metal chalcogenide, as in Scheme 1. A σ-donor compound added to the system, an amine for example, preferentially coordinates to the metal dialkyl, thus preventing the group 16 hydride from sufficiently approaching the metal centre to react. Against such a mechanism is the small ratio of pyridine to Me_2Zn (0.3 : 1) which is required in order virtually to eliminate the prereaction during growth of ZnSe.[14] Also, gas-phase IR spectroscopic studies clearly show such adducts to be fully dissociated into their substituent parts in the gas phase, even at ambient temperatures.[16]

A second mechanism proposes the prereaction to occur through an initial step involving metal–carbon bond homolysis of the group 12 precursor in the cold zone of the reactor cell, leading to the formation of radical intermediates. Radicals

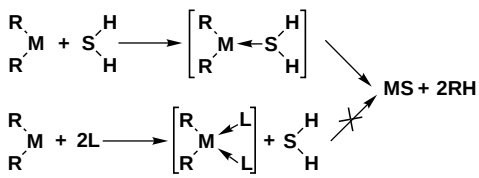

Scheme 1 Simple adduct 'blocking' mechanism. M = Cd or Zn, R = alkyl group, L = σ-donor group.

generated ($RM^{\bullet}$ and $R^{\bullet}$, M = Cd or Zn) would be highly reactive and rapidly react with other molecules present in the vapour phase, *i.e.* the group 16 hydrides or their radical fragments ($HS^{\bullet}/HSe^{\bullet}$) thus inducing a radical chain reaction and the eventual formation and precipitation from the gas-phase of a solid deposit. It has been postulated that in the presence of strong σ-donor compounds highly reactive metal-containing radical intermediates may be stabilised or trapped, so that the radical chain reaction is terminated when the oligomer species formed are still small and volatile enough to pass on into the hot zone of the reactor before precipitation of a solid occurs. However, initial metal–carbon bond homolysis in the cold zone of the reactor seems highly unlikely when one considers that metal alkyls have high thermal stability even in the presence of a reducing gas such as H_2.[17–20]

An extension[4] to the first mechanism again proposes initial gas-phase addition between the hydride and the metal dialkyl, followed by the reductive elimination of a saturated hydrocarbon leading to formation of [RMEH] (M = Cd or Zn, E = S or Se) as an intermediate. Instead of now simply undergoing a second reductive elimination to give ME, the intermediate, [RMEH], donates through the group 16 centre to a second metal dialkyl molecule which upon reductive elimination of RH leads to [RMEMR]. This leads, after a further group 16 hydride coordination and reductive elimination of RH, to the formation of the species, $[R(ME)_2H]$. Further propagation leads to oligomers of general formula $[R(ME)_xH]$, as shown in Scheme 2. The addition of a strong σ-donor to the gaseous system, may preferentially coordinate to the terminal Lewis-acidic metals and terminate chain propagation at a sufficiently early stage that the oligomers remain volatile enough to be transported to the growth zone. The last two mechanisms both proceed through the formation of oligomers of the type $[R(ME)_xH]$, and offer an explanation as to why σ-donor compounds are not required to be added in stoichiometric amounts to reduce or virtually eliminate prereaction, *i.e.* only binding to terminal metal centres within the oligomer units is required in order to terminate chain propagation.

It is known that the colour of some semiconductor materials, if they consist of particles in the nanometre size range, is dependent on particle size, for example, the colour of Cd_3P_2 changes from black (macrocrystalline) through brown (30 Å particles), red, orange, yellow to white (15 Å) as the particles become smaller.[21,22] A similar change in colour of the deposit when pyridine is added to a gas stream containing Me_2Cd and H_2Se has led us[23] and others[15] to propose an alternative explanation for the origin of the prereaction and its suppression by σ-donors. The σ-donor compound might bind to the surface of particles growing in the gas phase, inhibiting further particle growth and, in some cases, prevent II–VI material from precipitating from the gas phase.

Here, we report studies on the nature of the deposits obtained from gas-phase reactions between Me_2M and H_2E and how they are affected by the presence of pyridine, the temperature of mixing and the nature of the carrier gas, as well as on the nature of M and E. Preliminary reports of some of these studies have been communicated.[24,25]

Experimental

Dimethylcadmium and dimethylzinc were prepared and purified as described previously[26] and pyridine (Aldrich) was dried and distilled (over CaH_2) prior to use. Hydrogen sulfide (neat) was used as supplied by Matheson Gas Products along with hydrogen selenide supplied by Air Products. Helium and argon (BOC), used as the carrier gases, were purified by passing through two consecutive columns (2.5 cm × 80 cm) packed with Cr^{2+} on silica. Hydrogen used as a carrier gas was purified by passing through a Hewlett Packard oxygen scrubber prior to use.

Microanalytical data were obtained at the University of St. Andrews. Analysis of samples by powder X-ray diffraction was carried out on a STOE STADI/P diffractometer using Cu-Kα radiation. Transmission electron micrographs were obtained at the University of St. Andrews on a Phillips EM 301 microscope and at Glasgow University on a JEOL 1200 EX operated at 120 keV with a point resolution of 0.3 nm or an ABT 002B operated at 200 keV with a point resolution of 0.18 nm. Photoacoustic spectra were obtained on a OAS 400 photoacoustic spectrometer, with the band-gap of the deposits calculated from the knee at the top of the band edge in the spectra.[27]

Particle sizes were determined from the line broadening of PXRD patterns using a modification of Scherrer's formula,[28] as previously detailed.[29] Calculations on all samples were carried out using the same reflection (110) because this reflection did not overlap with neighbouring peaks when broad. Particle sizes were also determined from elemental analysis by assuming deposits consisted entirely of spherical particles of hexagonal material with each surface metal atom bound to a pyridine molecule; or by direct measurement of individual particles from transmission electron micrographs.

Preparation and collection of prereaction material

A schematic diagram of the experimental set up is shown in Fig. 1. The prereaction experiments were conducted at just above atmospheric pressure (101 350 Pa). Carrier gases containing specific gas-phase concentrations of reactants (Me_2Cd, Me_2Zn, H_2S, H_2Se and pyridine) were allowed to meet at the same point along a horizontal quartz tube which was heated, when required, by means of a ceramic tube furnace. Effluent

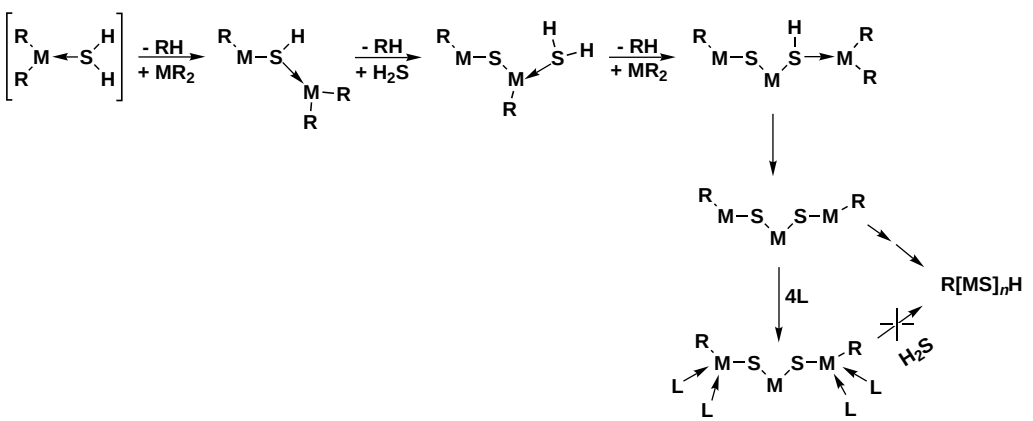

Scheme 2 Chain extension mechanism. M = Cd or Zn, R = alkyl group, L = σ-donor group.

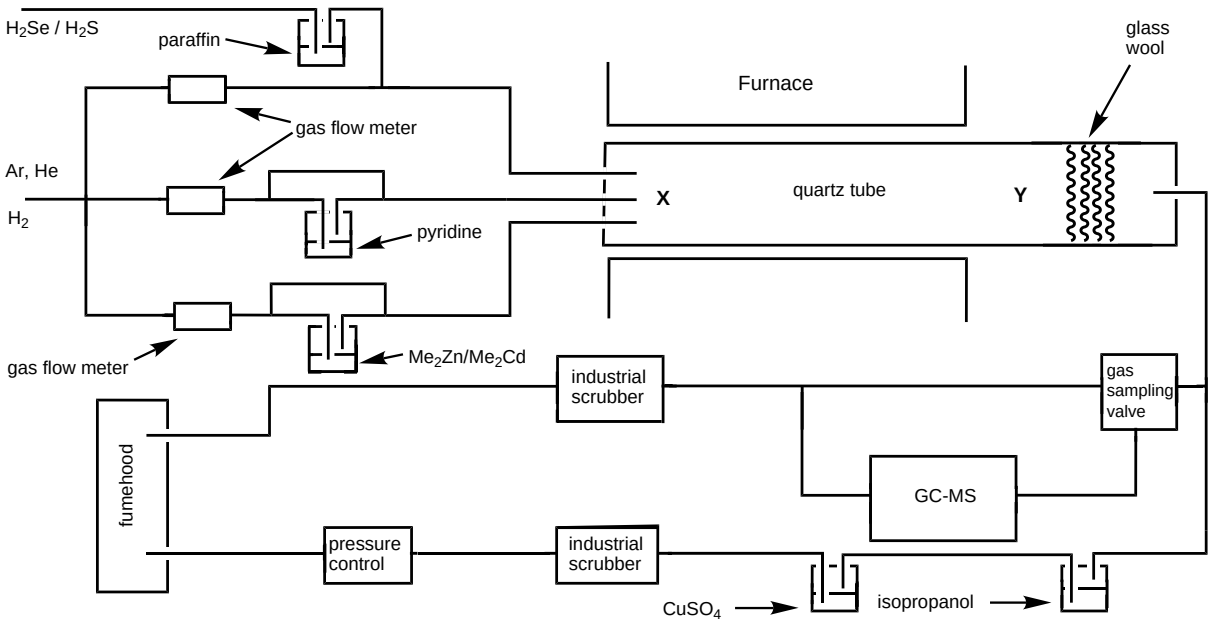

Fig. 1 Schematic diagram of the experimental set-up used in the preparation of semiconductor deposits

gases containing unused reactants and any volatile products were passed through neutralising solutions followed by an industrial scrubber before being released into a fumehood. For specific CdS experiments effluent gas was diverted *via* a gas sampling port to a gas chromatograph (HP 5890)–mass spectrometer (HP 5972 series mass selective detector) for analysis. Total gas flows were in the region of 600–2000 cm^3 min^{-1}, the gas-phase concentration of H_2S/H_2Se was maintained in a 30-fold excess to that of the metal dialkyl (range for Me_2Cd $1.2–9.2\times10^{-4}$ mol dm^{-3}, for Me_2Zn $3.9\times10^{-4}–2.1\times10^{-3}$ mol dm^{-3}) at the mixing point, depending on the ratio of pyridine to metal dialkyl used. The ratio of pyridine to metal dialkyl was varied by varying the rate of carrier gas flow through the bubblers of pyridine and metal dialkyl.

Results and Discussion

Techniques

The deposits obtained from the reaction of Me_2M (M = Cd or Zn) with H_2E (E = S or Se) in the presence or absence of pyridine in helium, argon or hydrogen gas at room temperature give broad X-ray patterns indicating that the deposits contain particles in the 1–50 nm range. The average sizes have been determined using analysis of the line broadening of the 110 line as this is present in both the cubic and hexagonal phases and is far enough away from neighbouring peaks not to overlap when broad. However, the X-ray patterns also give some information about the crystal quality in terms of the presence of distortions, preferred orientation, twinning, *etc*. We have also used microanalytical data to determine approximate average particle sizes by assuming that each particle is a sphere of hexagonal material with each surface metal atom bound to one pyridine molecule. This technique correlates well with the average particle diameter determined from PXRD in some cases but in others the correlation is poor, suggesting that, in some cases, not every surface atom is bound to a pyridine. We have also examined some of the deposits by TEM and find that there is a good correlation between the particle size obtained from the PXRD data and the average particle size obtained from TEM. Using HRTEM, we have studied individual particles and find that under certain conditions, polytypism or ordered arrays of quantum dots can be observed. We discuss these studies in greater detail later.

Gas-phase (He) reactions of Me_2M (M = Zn, Cd) with H_2S and Me_2Cd with H_2Se

Me_2Cd/H_2S. Me_2Cd reacts with H_2S in the gas phase at room temperature to give a deposit which shows a broad PXRD pattern (see Fig. 2). The pattern shows that the major phase present is hexagonal CdS (three reflections near $2\theta = 27°$, absence of reflection at 31.7°) but the absence or severe broadening of the 101, 102, and 103 reflections at $2\theta = 28.2$, 36.5 and 47.8° suggest that the registry in the 002 direction is poor and is characteristic of stacking faults along this axis.[30]

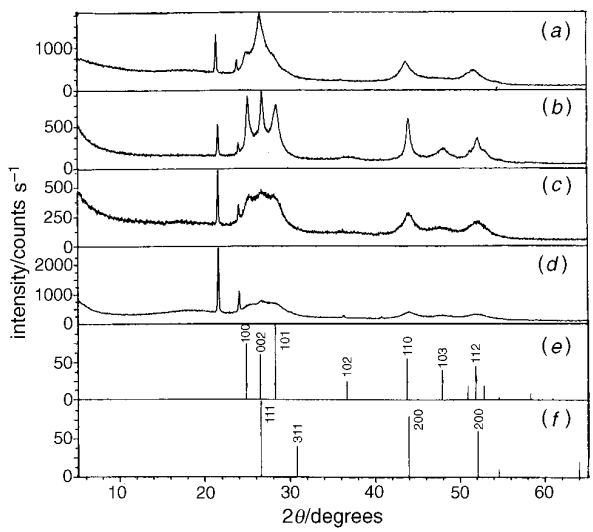

Fig. 2 X-Ray powder diffraction pattern of the CdS deposited during gas-phase mixing at ambient temperature of a 30:1 molar ratio of H_2S and Me_2Cd when (*a*) in the absence of pyridine (py), (*b*) py:Cd = 1:20, (*c*) py:Cd = 3:5 and (*d*) py:Cd = 2:1. Standard X-ray powder diffraction patterns of the (*e*) Greenockite and (*f*) Hawleyite phases of CdS. The peaks at $2\theta = 21$ and 24° arise from impurities in the vaseline support.

Table 1 Dependence of CdS particle size and band-gap on the concentration of pyridine (py) and the temperature at which the gas-phase reactants are mixed

py/Cd ratio[a]	temperature/°C	calculated diameter/nm		band-gap[c]/eV
		PXRD[a]	EA[b]	
0	25	6.1	—	—
0.05	25	16.0	14.7	2.44
0.16	25	9.8	10.5	2.51
0.3	25	7.0	8.4	2.54
0.6	25	6.9	9.5	2.49
1.0	25	4.4	6.2	2.64
2.0	25	4.6	6.7	—
2.0	50	12.9	—	2.47
2.0	100	23.1	—	2.35
0.05	150	38.4	—	—
0.3	150	35.4	—	—
0.5	150	39.2	—	—
2.0	150	37.6	—	2.35
2.0	200	38.3	—	2.31

[a]PXRD = Powder X-ray diffraction, [b]EA = Elemental analysis. [c]From photoacoustic spectroscopy.

Addition of a small amount of pyridine causes a slight increase in the average particle size (sharper PXRD patterns) but the crystal quality is greatly improved, as indicated by the appearance of the 101, 102 and 103 reflections [Fig. 2(*b*)] and the more similar line broadening for the remaining reflections to one another. We note that these 101, 102 and 103 reflections are still somewhat broader than the other reflections and have calculated that the crystal domains are non-spherical, by using Scherrer's formula on the 103 reflection which gave smaller values than the 110 reflection.

When the gas-phase molar ratio of pyridine to Me_2Cd is increased from 1:20 to 2:1 the particles of which the deposited material consists decrease in size as shown by PXRD, elemental analysis (Fig. 2 and Table 1) and direct inspection of TEM micrographs,[24] becoming smaller than those obtained in the absence of pyridine once the py:Cd ratio is 0.6:1. Also, at ambient temperatures, as the gas-phase concentration of pyridine is increased, the colour of the deposit undergoes a gradual change, from dark orange to pale yellow. This colour change is due to a size quantization affect. and should be associated with an increase in band-gap.[21,22] The change in the band-gap was determined by photoacoustic spectroscopy[27,31] measurements, which show the band-gap to increase from 2.44 to 2.64 eV as the ratio of pyridine to Me_2Cd in the gas phase was increased from 1:20 up to 1:1 (Table 1). The band-gap of bulk hexagonal CdS is 2.42 eV.[32] At low concentration, pyridine dramatically improves the crystal quality in the deposits, although some relative line broadening is still present, whilst at higher concentrations it inhibits the particle growth as indicated by a broadening of the PXRD diffraction patterns.

At a fixed gas-phase ratio of pyridine to Me_2Cd (2:1) the PXRD patterns become sharper with increasing temperature (as shown in Fig. 3). Elemental analysis showed that samples obtained above 100 °C contain very little pyridine. Calculations of particle size using Scherrer's formula (Table 2) suggest that the particles formed are large, outside the nanometre size range, with a sample of bulk CdS giving a PXRD pattern with similar peak width. A study by HRTEM on a deposit obtained with a 2:1 pyridine:Me_2Cd ratio at 200 °C, on a sample taken from near the precursor gas inlets, marked X on Fig. 1 (sample A) and on a sample of deposit which had drifted out of the hot zone of the reactor at point Y on Fig. 1 (sample B) was carried out. The samples were prepared for HRTEM by making a slurry in water and drying one drop of the slurry on a carbon film support on an electron microscope grid.

Low-resolution images of A (*ca.* 206 000 ×) show well

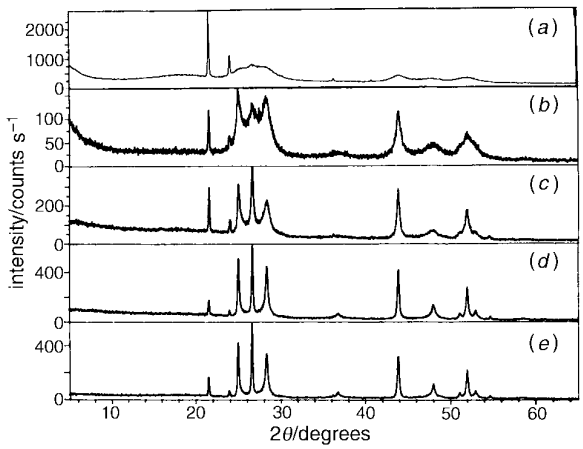

Fig. 3 X-Ray powder diffraction pattern of the CdS deposited during gas-phase mixing of H_2S, Me_2Cd and pyridine (30:1:2) at (*a*) 25 °C, (*b*) 50 °C, (*c*) 100 °C, (*d*) 150 °C and (*e*) 200 °C

Table 2 Dependence of ZnS particle size on the concentration of pyridine (py) and the temperature at which the gas-phase reactants are mixed

py/Zn ratio	temperature/°C	calculated diameter/nm	
		PXRD[a]	EA[b]
0.20	25	5.0	13.5
0.40	25	4.5	10.6
0.8	25	3.0	4.3
2.0	25	2.3	3.1
2.0	50	4.1	—
2.0	100	6.9	—
2.0	150	22.9	—
0.1	200	43.4	—
0.3	200	31.4	—
0.5	200	27.8	—
1.0	200	29.9	—
2.0	200	29.8	—
2.0	300	31.9	—

[a]PXRD = Powder X-ray diffraction. [b]EA = Elemental analysis.

developed crystals of good crystalline quality up to 500 nm in size; however, calculations from PXRD patterns suggest that the crystallites are no more than 5 nm in size. At higher resolution [Fig. 4(*a*)] extensive dislocations can be seen, a study of different areas within the same crystal reveals lattice spacing corresponding to either or both hexagonal and cubic CdS. Moreover, crystals in sample A are large but contain stacking faults in the 002 layer plane, with the fault lines being *ca.* 1–4 nm apart. One could view these large crystals [as shown schematically in the insert to Fig. 4(*a*)] as being made up of stacks of smaller crystals, slightly misaligned relative to one another. However, deposits prepared at 100 °C or above give similar band-gap measurements close to that of bulk CdS (2.42 eV) suggesting that this view that the large crystals are just a stack of smaller one does not apply as far as quantization effects are concerned.

Low-resolution images of B (*ca.* 50 000–300 000 ×), are similar to A, showing faceted objects up to 1 μm in size, consisting of individual crystals, having intimate contact with one another, of up to 0.2 mm in size. As in sample A, these crystals contain numerous distortions which could arise from multiple twinning, stacking faults or multiple shear structures. Regular lines of contrast running across the crystal, being too big to be lattice planes, are typical of multiple stacking faults. Other crystals show many irregular contrast lines with no consistency in direction or breath of contrast. Higher resolution images (*ca.* 3 900 000 ×), as in Fig. 4(*b*), show continuous lattice planes

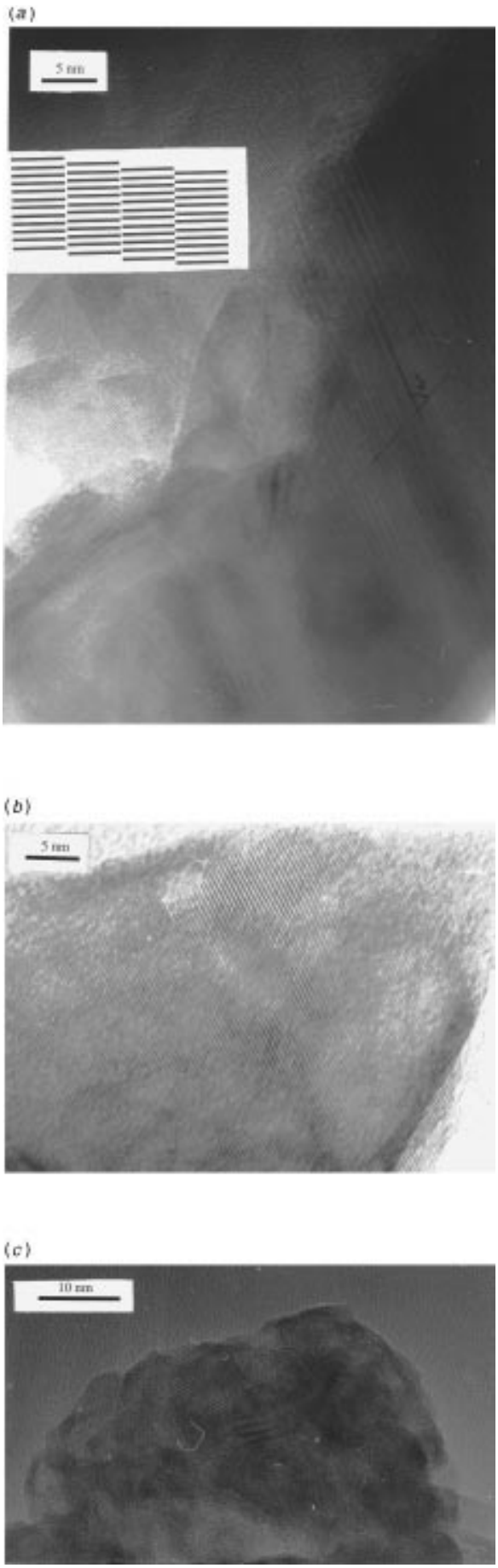

extending over 50 nm, but as in A, these show regions where contrast is lost indicating some bending of the lattice. Measurements of the lattice dimensions, especially for sample A, give some spacings which do not correspond to those of hexagonal CdS, even when errors associated with a visual measurement and inaccuracies in magnification are taken into account. This suggests that there are significant numbers of stacking faults within the crystal.

It appears that the growth of these large crystals is rapid and occurs entirely while suspended in the gas phase, close to the gas inlet of the reactor, and not from aggregation of small crystals which then anneal to form large ones. Evidence for the cessation of particle growth once the deposit has precipitated from the gas phase was obtained by taking a sample of the deposit obtained from H_2S, pyridine and Me_2Cd (30 : 2:1) at 25 °C and placing it at 160 °C for 8 h. Elemental analysis, on the resulting solid (sample C), showed most of the pyridine still remained within the sample and a comparison of PXRD patterns of the original deposit with sample C showed them to be similar, the latter having a slightly sharper peak profile. For the original deposit the particle size calculated from elemental analysis is 6.7 nm and that from PXRD (using Scherrer's formula) 4.6 nm, for C the calculated particle sizes from elemental analyses and PXRD are 11.4 and 5.6 nm respectively. The discrepancy between the particle sizes calculated from elemental analysis is due to some loss of pyridine at high temperature leaving vacant sites; however, these results strongly suggest that particles do not anneal into bigger crystals once formed. The best evidence that small crystallites do not anneal to form large crystals is from an HRTEM study of sample C. Sample C was prepared for HRTEM studies in a similar manner to A and B, low resolution images (200 000–300 000 ×) showed large 100–1000 nm spherical agglomerates, with none of the faceting observed in A or B. At higher resolution (2 000 000 ×), it can be seen that these agglomerates are made up of small crystals each of which is randomly oriented with respect to one another [Fig. 4(*c*)]. It can be seen that the small crystals have generally well ordered lattice planes with sizes in the range 1–10 nm.

Further evidence for suppression of particle growth by the binding of pyridine to surface metal atoms was obtained from solid-state ^{113}Cd and ^{13}C NMR, ^{13}C confirmed that pyridine was the only organic compound (compound containing carbon) within the deposits produced in the presence of pyridine and that the pyridine was coordinated through the nitrogen atom to surface bound cadmium atoms. A sample prepared in the absence of pyridine showed (^{13}C NMR) no methyl groups or other organics to be present; however, all samples were exposed to air prior to analysis, thus any residual methyl groups may have been hydrolysed. Cross-polarisation solid-state ^{113}Cd NMR gave one broad peak at *ca.* 502 ppm relative to hydrated cadmium chloride for a sample deposited in the absence of pyridine and for a deposit obtained in the presence of pyridine (1 : 2 Me_2Cd to pyridine ratio) a large peak at *ca.* 502 ppm along with a much smaller peak upfield at *ca.* 520 ppm. We propose that this small peak arises from Cd atoms on the surface of the particles and the shift to higher field is consistent with their being bound to the pyridine molecules.

Fig. 4 HRTEM images of CdS deposited when using a pyridine to Me_2Cd ratio of 2 : 1 at a temperature of 200 °C: (*a*) sample A taken from the hot zone of the reactor (inset: schematic illustration of stacking faults along the 002 layer in the hexagonal phase or the 111 in the cubic phase, which lead to the variations in contrast, not to scale); (*b*) sample B (high magnification) taken from downstream of the hot zone of the reactor; (*c*) CdS deposited when using a pyridine to Me_2Cd ratio of 2 : 1 at a temperature of 25 °C then heated to 160 °C for 6 h, sample range C.

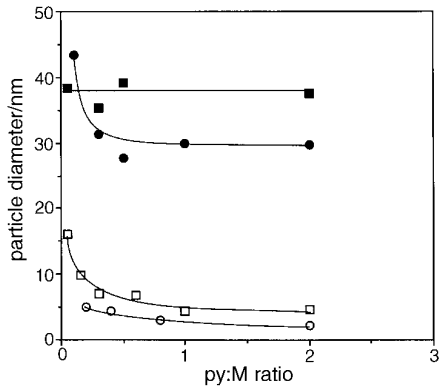

Fig. 5 Variation of average particle size (determined by PXRD) with py : M ratio (M = Cd or Zn) at 25 °C, ZnS (○) and CdS (□), at 200 °C, ZnS (●) and at 150 °C, CdS (■)

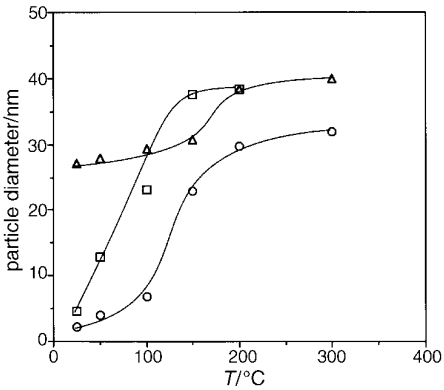

Fig. 6 Variation of average particle size (determined by PXRD) with gas-phase mixing temperature at py : M = 2 : 1. ZnS (○), CdS (□), ZnSe (△).

Me_2Zn/H_2S. The reaction of Me_2Zn with H_2S in the absence or presence of pyridine gave similar results to those of CdS, with small amounts of pyridine improving the crystal quality while increasing the average particle size. The average particle size, determined from PXRD and EA, again decreased as the gas-phase concentration of pyridine was increased at a fixed reaction temperature. The particle size also increased with increasing temperature at fixed gas-phase precursor concentrations (Table 2).[25]

A comparison of the dependence of average particle size upon the py : Me_2M ratio at ambient temperature and higher temperatures is shown in Fig. 5 and a comparision of the particle size (at fixed py : Me_2M ratio of 2 : 1) at varying temperature in Fig. 6. In general, the particles of ZnS are smaller than those of CdS under a given set of conditions. We attribute this to the known stronger bond of zinc than of cadmium to nitrogen donors.[33] At ambient temperature the particle size for CdS is more sensitive to the py : Me_2M ratio than ZnS. Conversely, as the temperature is raised, the particle size for CdS becomes independent of temperature at a much lower temperature than does that for ZnS. Elemental analyses on both CdS and ZnS deposits formed at temperatures above 100 °C reveal the presence of very little residual pyridine, indicating the lability of the metal–nitrogen donor–acceptor bond at higher temperatures, leading to deposits with higher average particle sizes.

Me_2Cd/H_2Se. For the gas-phase reaction between Me_2Cd and H_2Se the deposit which formed underwent a much more pronounced change in colour than when using H_2S. However, much higher gas-phase concentrations of pyridine were required to produce particles of corresponding size (Table 3). In the absence of pyridine a black deposit formed along the entire length of the quartz tube. Calculations using PXRD data, indicated the particles to be *ca.* 10 nm in diameter. The PXRD pattern [Fig. 7(*a*)] in the absence of pyridine is more characteristic of the cubic phase than the hexagonal one with no *hkl* reflections for the 103, 102 and 101 reflections, with the 100 reflection being at the same 2θ value as one of the peaks from the Vaseline support making it difficult to establish the intensity of this peak. The uncharacteristic PXRD patterns may be due to a high degree of defects within the particles. The loss of 103, 102 and 101 reflections along with the large intensity of the 002 reflection suggest a large number of 002 planes or a high number of stacking faults perpendicular to this plane. A study of PXRD patterns of the hexagonal and cubic phase of nanoparticles of CdSe (3.5–4.0 nm) by Bawendi *et al.*[33] has shown that a small number of stacking faults within a particle has a dramatic effect on the overall appearance of the PXRD pattern. Moreover, the occurrence of approximately

Table 3 Dependence of CdSe particle size and colour on the concentration of gas-phase pyridine (py) at ambient temperature

py/Cd ratio	calculated diameter/nm PXRD[a]	colour
0.0	9.7	black
0.5	13.9	dark brown
1.0	13.9	dark brown
2.0	12.5	brown
4.0	11.5	maroon
16.0	9.2	red–brown
50.0	6.2	red
150.0	5.0	yellowish–red

[a]PXRD = powder X-ray diffraction.

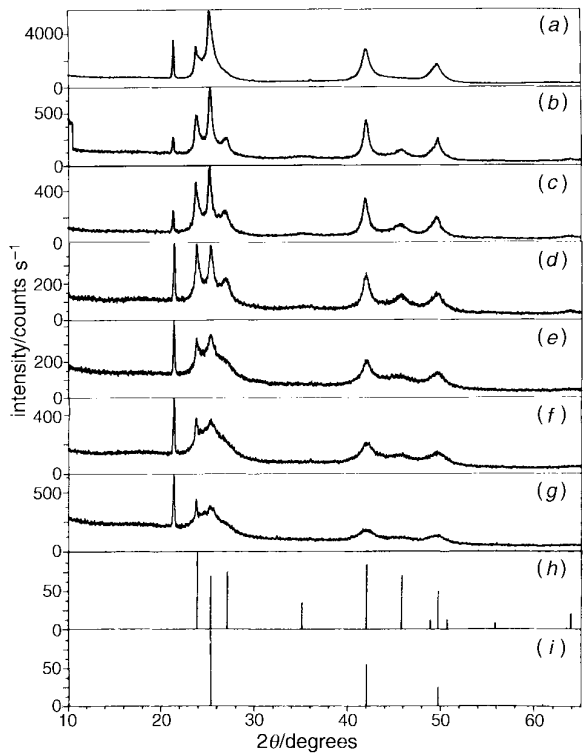

Fig. 7 X-Ray powder diffraction pattern of the CdSe deposited during gas-phase mixing at ambient temperature of a 30 : 1 molar ratio of H_2S and Me_2Cd when (*a*) in the absence of pyridine, (*b*) py : Cd = 1 : 1, (*c*) py : Cd = 2 : 1, (*d*) py : Cd = 4 : 1, (*e*) py : Cd = 16 : 1, (*f*) py : Cd = 50 : 1, (*g*) py : Cd = 150 : 1, with standard X-ray powder diffraction patterns of the (*h*) hexagonal and (*i*) cubic phases of CdSe

Table 4 Dependence of ZnSe average particle size (from PXRD)[a] on the concentration of pyridine and the temperature at which the gas-phase reactants are mixed

py/Me_2Zn ratio	temperature/°C	particle diameter/nm
1.0	25	27.2
1.5	50	28.0
1.0	100	29.3
1.0	150	30.8
1.0	200	38.4
1.0	300	40.0
0	25	11.9
0.05	25	29.0
0.2	25	31.0
0.25	25	30.0
0.6	25	43.5
0.8	25	23.1
1.5	25	30.9

[a]PXRD = powder X-ray diffraction.

one stacking fault every eight planes in a particle consisting of the hexagonal phase can cause the PXRD pattern to resemble that of the cubic phase.

In contrast, deposits prepared in the presence of pyridine, as judged from PXRD patterns, even at gas-phase concentrations as low as 2:1 Me_2Cd:py contain primarily the hexagonal phase although the 101, 102 and 103 reflections are substantially broader than other reflections, indicating poor crystal quality arising from stacking faults or other defects, such as multiple twinning.

As the gas-phase concentration of pyridine is increased, the colour of the material deposited changes dramatically as indicated in Table 3. Particle sizes calculated from elemental analysis were up to five times larger than values obtained from PXRD, suggesting that not all surface cadmium sites are coordinated to pyridine.

Gas-phase reactions between Me_2Zn and H_2Se in the presence of pyridine using helium and hydrogen as carrier gas

Gas-phase reactions between Me_2Zn and H_2Se, under identical conditions to those used for CdS, ZnS and CdSe at ambient temperatures, led to the formation of a pale yellow deposit, with the colour of the deposit changing to white only when a 2:1 or greater pyridine to Me_2Zn molar ratio was used. Calculations from PXRD patterns gave average particle sizes in all samples when using py:Zn ratios $<2:1$ to be between 25.0–40.0 nm (Table 4); elemental analysis results show the presence of very little organic material (pyridine) in the deposits. However, at a ratio of 2:1 (py:Zn) very substantial peak broadening occurred in the PXRD pattern, Fig. 8, (too broad for an accurate size determination) suggesting the formation of very small particles. Like ZnS and CdS, increasing temperature at a fixed gas-phase precursor concentration (ratio py:Me_2Zn = 2:1) led to sharpening of peaks in the PXRD patterns and thus large particles in the deposit. Compared with both ZnS and CdS, the ZnSe particle size is less sensitive to temperature (Fig. 6), however, the temperature at which pyridine ceases to have any effect (between 100 and 150 °C) seems to be similar for all three compounds. A study by high-resolution transmission electron microscopy (HRTEM) on a sample prepared in the absence of pyridine, sample D; a sample prepared using a gas-phase pyridine:Me_2Zn ratio of 1:5, sample E and a sample prepared using a ratio of 2:1, sample F, revealed some quite dramatic results.

Samples D–F were prepared for HRTEM by forming a slurry with acetone and then allowing a drop of slurry to dry on a carbon film, supported on a copper grid or were embedded in a polymeric matrix, slurried in acetone then placed on a carbon grid. Sample D consisted of a homogeneous array of polycrystalline particles with diameters *ca.* 150 nm, Fig. 9(*a*).

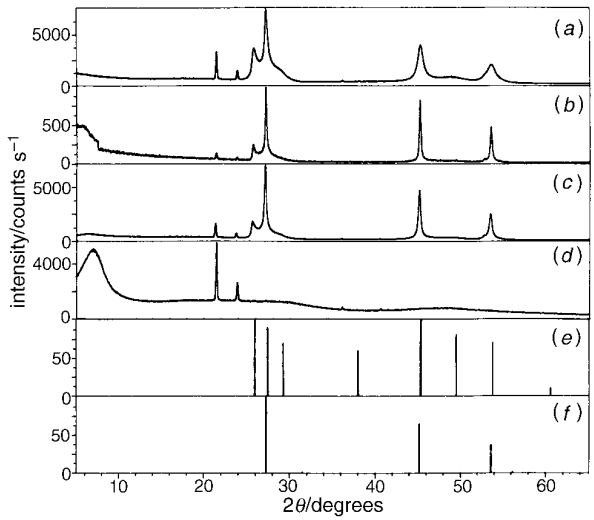

Fig. 8 PXRD patterns of the ZnSe deposited during gas-phase mixing at ambient temperature of a 30:1 mole ratio of H_2Se and Me_2Zn when in helium (*a*) in the absence of pyridine, (*b*) py:Zn = 3:5, (*c*) py:Zn = 1:1, (*d*) py:Zn = 2:1. Standard PXRD patterns of (*e*) hexagonal and (*f*) cubic ZnSe are also shown.

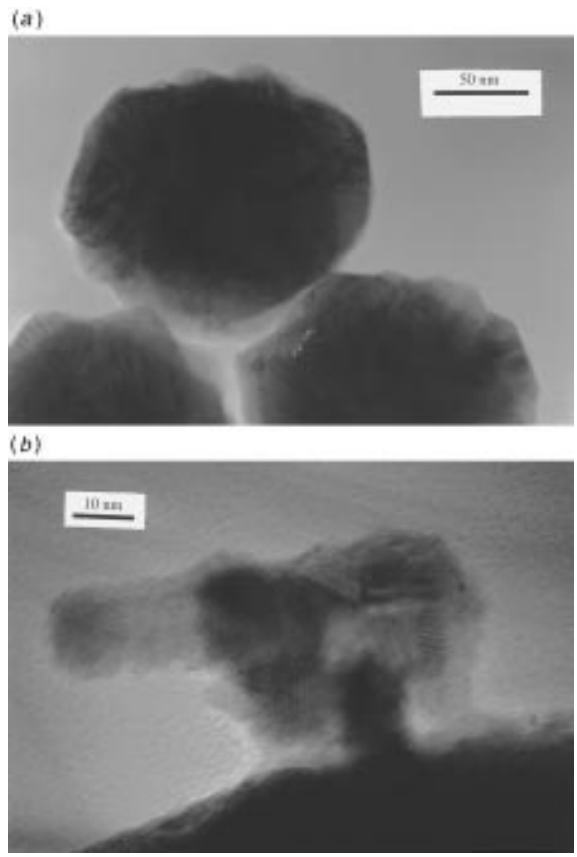

Fig. 9 HRTEM images and ZnSe deposited at ambient temperature from H_2Se and Me_2Zn: (*a*) in the absence of pyridine, sample D; (*b*) H_2Se:Me_2Zn:pyridine = 30:5:1, sample E, showing an area containing smaller particles

At higher resolution two lattice distances >0.3 nm are visible (0.34 and 0.33 nm) whereas the cubic phase has only one spacing >0.3 nm, the particles are essentially the hexagonal phase. There is disorder at the edge of the crystal, which is typical of small particles where reconstruction may be taking

place making it partially crystalline. However, there are also stacking faults leading to multiple twinning, indicated by darker contrast areas in the TEM micrographs, which run through the particles and it is probably for this reason there is such a discrepancy between the particle size seen in the TEM and that obtained from PXRD pattern (11.9 nm) calculations. These disorders may explain why the 101, 102 and 103 hkl reflections are substantially broadened.

Sample E is similar in appearance to D, but the variation in crystal size is much greater with a range of sizes from 100 to 500 nm in diameter. There are also much smaller crystalline particles present with diameters in the range 20–40 nm [Fig. 9(*b*)]. These smaller particles project from the surface of the larger ones and appear to be highly crystalline. Moreover, it appears that each large particle is composed of one extensive crystal, similar to D, but coated with a layer of smaller crystals. For the small crystals, those that could be measured are of the hexagonal phase, and contain lattice distortions of all types, with no particular one predominating. Sample F contained a polymeric organic residue, probably from the pyridine, giving globular masses. At higher magnification, it was evident that the globular masses consisted of crystalline particles of *ca.* 4 nm in size although some are as big as 8 nm and others as small as 2 nm. Many crystals show well defined regular lattices but others are severely distorted. Due to masking by the organic material, it is not possible unambiguously to characterise the phase, however, lattice spacing measurements suggest that it is hexagonal since there are variations in the range 0.32–0.34 nm for different crystals.

It is evident from this study by HRTEM that the effect of pyridine was to increase the proportion of smaller crystals within the deposited material with all the ZnSe in sample F being in the form of small crystals. It is the extent of the largest crystalline domains within the large particles of a sample which probably determines the particle size calculated by PXRD patterns, since, being sharper, the diffraction peaks from these particles dominate the pattern. All samples with a ratio of $Me_2Zn : H_2Se < 2$ gave a similar PXRD pattern because larger crystalline particles were still present.

When using hydrogen, a gas-phase prereaction of Me_2Zn with H_2Se still occurred in the presence of pyridine at room temperature, albeit to a lesser extent. Calculations from PXRD patterns indicate that the average particle size within a deposit decreases with increased gas-phase concentrations of pyridine and the particle sizes are much smaller than in the analogous deposits when using helium. At a ratio of 2 : 3 (py : Zn) very substantial peak broadening occurred making it impossible to determine accurate particle sizes using Scherrer's formula. A study by HRTEM on a sample prepared in the absence of pyridine, sample G; a sample prepared using a gas-phase pyridine : Me_2Zn ratio of 1 : 5, sample H, and a sample prepared using a ratio of 2 : 1, sample I, revealed quite different results from those obtained when using helium as the carrier gas.

Sample G consisted of agglomerates, in the size range 5–25 nm, made up of crystalline particles 2–10 nm in diameter with well defined lattice fringes, having fewer stacking faults than in the deposit in sample D. The lattice fringes were less distinct than those in D, because of the smaller crystal size. Measurement of the fringes only showed a single spacing above 3 nm and electron diffraction gave a broad ring in the range 0.35–0.30 nm with spacings at 0.2 and 0.17 nm, common to both hexagonal and cubic phases. The presence of the cubic phase could not be ruled out because of the coincidence of lattice spacings, but the electron diffraction supports the presence of just the hexagonal phase. For sample H the presence of organic material (pyridine) could be seen in the form of globular masses (diameter 50–400 nm). Most contained ZnSe crystalline particles but some were just pure organic material. The detachment of pyridine from ZnSe particles may have occurred when preparing samples for HRTEM analysis (slurry with acetone). The agglomerates consist of small ZnSe particles with a relatively narrow size distribution (1–5 nm, mean 1.5 nm) randomly orientated with respect to one another (Fig. 10). The lattice images showed the lattice to be bent and twisted, the distortions being somewhat different from the dislocations and stacking faults seen in other samples and they are more likely to arise from turbostratic distortions.[34] The degree of disorder within the crystalline particles of H was much higher than that seen in samples E and G. Owing to the small size of the crystals and the high degree of imperfections it was impossible to judge the phase of the particles.

For the sample prepared with a py : Me_2Zn ratio of 2 : 1, sample I, there was a large quantity of organic material present which had the effect of obscuring the ZnSe from the electron beam. However, it was possible to see dark areas consisting of ZnSe particles in the size range 2–5 nm, slightly larger than in H. The resolution of the image was poor and the particles may be the same size as in H or even smaller. The PXRD patterns suggest that these particles (sample I) are smaller than those of sample H or have a higher degree of imperfection. From the small areas of micrographs having visible lattice fringes it is clear that the randomly oriented crystals are smaller and more uniform than in sample F. The electron diffraction pattern was nearly amorphous but the distances between the centres of the rings was *ca.* 0.01–0.03 nm which is different from the perfect hexagonal phase but does not correspond to the cubic phase either, indicating, as in the PXRD pattern, many distortions within the crystals.

Hydrogen has the effect of forming smaller nanoparticles with a more uniform distribution within a deposit, however, the distortions within the particles increase when using hydrogen in the presence of increasing gas-phase concentration of pyridine. These studies also confirm that the particle sizes calculated from PXRD patterns using Scherrer's formula can only be used as a rough indication of particle size.

When the reaction of Me_2Zn with H_2Se in hydrogen in the presence of pyridine was carried out at a higher temperature, the prereaction was almost completely eliminated with no deposit being observed in the hot zone and only traces of

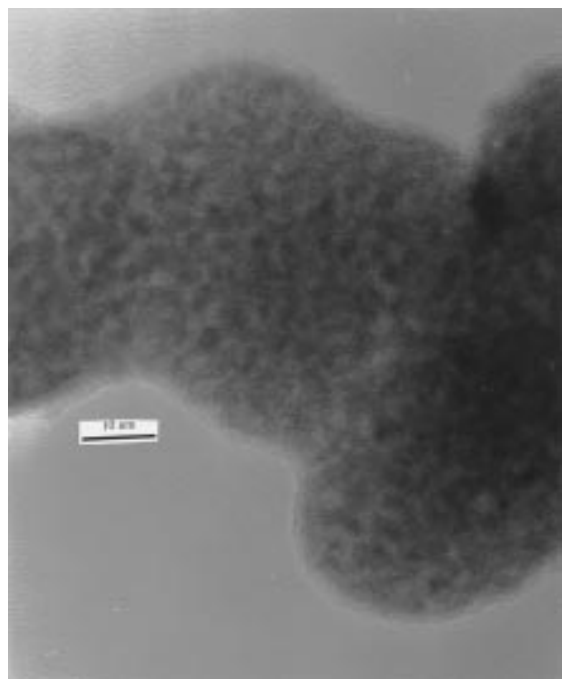

Fig. 10 HRTEM image of ZnSe deposited at ambient temperature $H_2Se : Me_2Zn$: pyridine = 30 : 5:1, sample H, showing nanoparticles of narrow size distribution

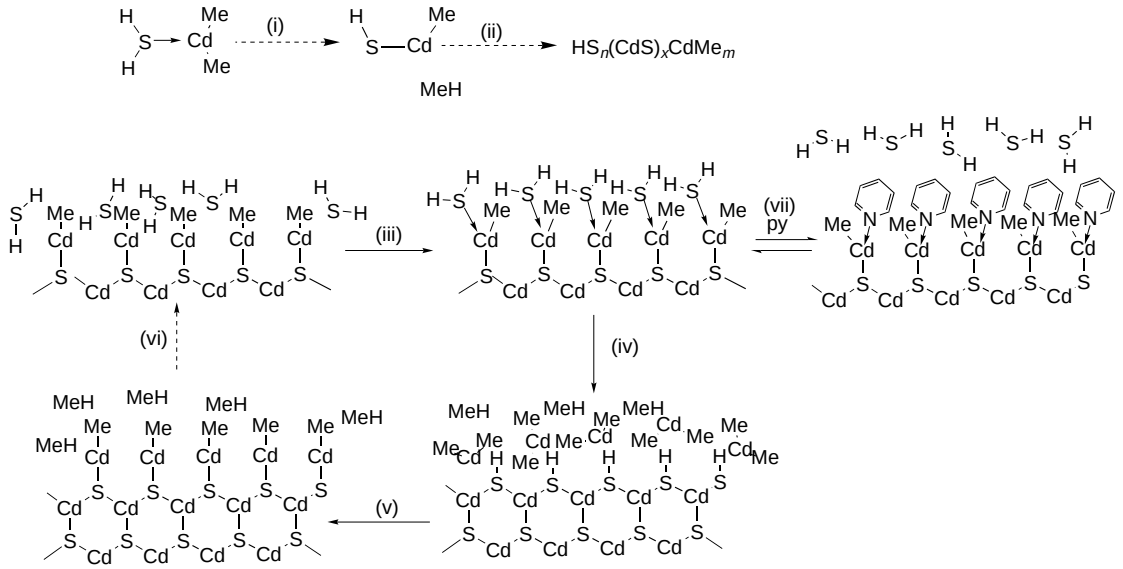

Fig. 11 Schematic representation of the origins of prereaction and its suppression by the presence of pyridine

deposit in the mixing zone and in the colder exit zone. In addition, material was deposited in parts of the apparatus well downstream of the heated tube (flow meters *etc.*). This behaviour contrasts with that of all other systems reported in this paper, since for them the particle size tends to increase as the temperature is increased. The observation of deposits well downstream of the reactor suggests that volatile species are produced, but that they are unstable with respect to a slow decomposition or reaction with H_2Se. We have attempted to identify the volatile component using GC–MS, but no new species (*i.e.* other than methane, pyridine and H_2Se) were observed.

Analysis of gaseous products from reaction of Me_2Zn, H_2S and pyridine

Mixing Me_2Zn and pyridine (py : Me_2Zn = 2 : 1) in the absence of H_2S produced white needle-shaped crystals of what was shown by ^1H NMR spectroscopic analysis to be the bispyridine adduct [$Me_2Zn{\cdot}2py$]. GC–MS revealed the presence of only Me_2Zn and pyridine in the gas phase, with no indication of any gas-borne adduct, which is in accord with IR spectroscopic studies.[16] When H_2S was added to the gas stream (H_2S : Me_2Zn : py = 30 : 1 : 2), GC–MS analysis of the exhaust gas from the quartz tube revealed the presence of methane, H_2S and pyridine. No oligomers of the type [$Me(ZnS)_mH]{\cdot}n$py were observed, however, such species may rapidly attain a high molecular mass, making them too large to stay gas borne let alone pass through a GC column. These results suggest that a reaction between an associative $MMe_2{-}SH_2$ complex occurs with the release of methane, due to the effective elimination of alkyl groups in the presence of the acidic hydrogen atoms of the H_2S, any suppression of the prereaction occurs after this initial step rather than by an adduct blocking mechanism.

Mechanism for nucleation and suppression of prereaction

Taking the results discussed above together, we can propose that the particulate matter seen both here and under more typical MOVPE growth conditions forms through a process of growth and nucleation within the gas phase. In the absence of a Lewis base, the growth occurs by the mechanism represented schematically in Fig. 11(i–vi). Initial association between MMe_2 and H_2S leads to the formation of $[RMSH]_2$ which grows rapidly into clusters of the type $HS_n(MS)_xMMe_m$ consisting of a central MS core with SH and MMe fragments on the surface of the particles, suspended within the carrier gas. Gas-phase H_2S now reacts with residual surface bound M—Me fragments leading to methane elimination and the formation of new S—H sites which in turn react with gas-phase Me_2Zn leading to the formation of new zinc/cadmium sites on the continuously growing particles. Replacement of alkyl groups by sulfur atoms, which are more electronegative, increases the Lewis-acid strength of the surface metal atoms. As the size of the cluster increases, two things happen. Firstly the surface metal sites become more Lewis acidic in nature favouring the binding of pyridine over that of H_2S and hence displacing equilibrium (vii) of Fig. 11 towards the pyridine bound form. Under some conditions of pyridine concentration, temperature and metal, this will terminate the growth. Secondly, the proportion of metal atoms available for coordination (those on the surface of the growing particle) reduces as the particle grows (*i.e.* the effective pyridine : M ratio increases).

The role of pyridine is, then, to terminate the particle growth and the efficiency with which it does this will depend upon the equilibrium constant for displacement of H_2E from the growing particle by pyridine [Fig. 11(vii)] leading to gowth termination† and the rate of reaction of surface-bound H_2E with surface methyl groups [Fig. 11(iv)], leading to growth.

We have previously proposed that for the systems involving H_2S, the position of the equilibrium involving displacement of H_2S by pyridine [Fig. 11(vii)] is the controlling factor, with the harder nature of zinc than of cadmium[35] meaning that the equilibrium will lie further to the pyridine binding side for zinc, since pyridine is a harder Lewis base than H_2S. This accounts for the smaller particles of ZnS than of CdS obtained under identical conditions.

Furthermore, on raising the temperature it is anticipated that the equilibrium involving loss of pyridine from the surface of the particle and recoordination of H_2S [Fig. 11(vii)] will shift in favour of dissociation of the pyridine (since this reaction has a negative $\Delta S°$). This should lead to larger particles at higher temperature, as is observed. Increasing the amount of pyridine should shift the equilibrium [Fig. 11(vii)] in favour of the adduct leading to smaller particles, again as observed. The relative insensitivity of the particle size of ZnS to the

† Because the H_2E : pyridine ratio is generally $>15:1$, it is unlikely that pyridine will react faster with surface M atoms than H_2E.

py : Zn ratio at ambient temperature can be attributed to the equilibrium lying completely to the pyridine adduct once a particular ratio has been reached, whilst the insensitivity of the size of the CdS particles to temperature suggests that the pyridine adduct for M = Cd is completely dissociated for a py : Me_2Cd ratio of 2 : 1 above 150 °C. Finally, the fact that only small amounts of pyridine can have dramatic effects on the prereaction can be accounted for because only the surface metal atoms need to be coordinated to the pyridine to prevent further growth. If the equilibrium constant for Fig. 11(vii) is high, the ratio of py : Me_2M to prevent growth of particles beyond a particular size is equal to the ratio of the number of surface atoms to the total number of atoms; this drops rapidly as the particle size increases.

The results obtained in the growth of ZnS and CdS can be explained in terms of the equilibrium shown in Fig. 11(vii), and the different Lewis acidities of Zn and Cd. If this were the only controlling factor, one might expect at least as good control of particle size by pyridine in the growth of CdSe and ZnSe. Indeed it might be even better since H_2Se is a weaker Lewis base towards these metals than H_2S and hence should not compete so effectively with pyridine for coordination and growth. This is not the case and, indeed, pyridine has relatively poor control in these systems, especially ZnSe at room temperature. Certain observations lead us, therefore, to propose that the rate of loss of methane from the surface of the growing particle [Fig. 11(vi)] is more important in these systems. In particular, the ZnSe particles contain almost no pyridine and those of CdSe contain much less than one pyridine molecule per surface Cd atom. These observations suggest that pyridine is prevented from binding to the surface Cd atoms but this cannot be because of competitive binding of H_2Se, since H_2Se is a weaker Lewis base than H_2S.

The rate of elimination of methane is expected to depend on the relative acidity of H_2E and the bond polarity of Me—M. H_2Se is a much stronger acid (K_1 and $K_2 = 1.3 \times 10^{-4}$ and *ca.* 10^{-11} mol dm^{-3})[35] than H_2S (1.3×10^{-7} and 7.1×10^{-15} mol dm^{-3})[35] so that methane elimination should be faster for H_2Se than for H_2S. The Me—Zn bond is more polar than the Me—Cd (both δ^- on Me) so that the relative rates of methane elimination should be ZnSe > CdSe > ZnS > CdS. In the case of the sulfides, we have suggested that the rate of methane elimination is sufficiently low that the surface bound H_2S complex has a long enough lifetime for pyridine to displace H_2S and terminate growth [Fig. 11(vii)], this being more effective for Zn than for Cd because of the greater stability constant of the Zn—pyridine bond. For H_2Se, we propose that the rate of elimination of methane [Fig. 11(iv)] is so fast that pyridine cannot displace the H_2Se and therefore does not control the growth well except at high gas-phase concentrations. This will be especially the case for ZnSe, with the slightly lower rate of methane elimination for CdSe allowing some control by pyridine in this case.

In a hydrogen ambient rather better control of ZnSe growth is observed than in He. This is somewhat surprising, as is the observation that almost complete inhibition of the prereaction is observed both in MOVPE studies and by us at higher temperature. In the other cases, higher temperatures make pyridine less effective at controlling the particle growth.

One possible explanation is that H_2 can react with surface Zn—Me bonds on the growing particles to give methane and Zn—H. These Zn—H bonds are known to be relatively inert[17] and may react much less readily with H_2Se to eliminate H_2, slowing particle growth. Also, it has previously been reported that zinc hydride and EtZnH in pure pyridine react to form, in the case of zinc hydride, the complex bis(4-hydro-1-pyridyl)-zinc, with the hydride atom originally bound to the zinc transferring to the *para* position of the pyridine.[36,37] If a similar reaction occurs, in the gas phase, between surface Zn—H bonds of gas-phase particles and pyridine to form surface-bound complexes as shown in Fig. 12, the prereaction may well be inhibited because the interaction between the Zn atom and the pyridine is no longer that of a simple donor–acceptor complex, but similar to that in a zinc amide. The equilibrium for such a reaction may lie far over to the right and stop particle growth much more effectively than a dative bond between the zinc and pyridine.

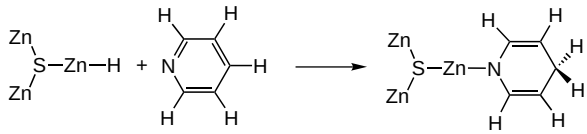

Fig. 12 Possible reaction of pyridine with a Zn—H bond on the surface of gas-phase ZnS particles

At higher temperatures, it may be that Me_2Zn, H_2 and pyridine react together to form [Zn(4-hydropyridyl)$_2$], a volatile amide precursor and that this is less reactive towards H_2Se so that it can be transported into the hot zone of the reactor and then allow growth only over the substrate. Other zinc amides have been shown to be effective MOVPE precursors for the growth of ZnSe using H_2Se.[38] We have attempted to observe such species using GCMS of the effluent from the tube, but have not succeeded. Indeed, the deposits downstream of the reactor suggest that whatever volatile species is formed is not indefinitely stable.

Conclusion

In the absence of pyridine, Me_2M (M = Cd or Zn) react with H_2E (E = S or Se) in a helium ambient to produce deposits in the nanometer size range of hexagonal ME, but with poor crystal quality. Addition of pyridine improves the crystal quality and at higher levels reduces the particle size. A rational mechanism for the inhibition of particle growth involving binding of the pyridine to the metal surface of particles growing in the gas phase is proposed and it is shown that the gas-phase concentration of pyridine, the temperature, the acidity of H_2E, the Lewis acidity of M and the nature of the carrier gas all affect the size of the particles and their crystal quality. Using both H_2 and pyridine has a particular dramatic effect on the size of particles of ZnSe grown and can provide a route to nanoparticles of ZnSe with relatively narrow size distribution. At higher temperatures, in hydrogen, pyridine almost completely eliminates the prereaction betwen Me_2Zn and H_2Se perhaps because a more stable zinc amide complex is formed.

We thank the EPSRC for financial support (N.L.P., *via* a ROPA award and D.F.F.).

References

1 S. Fujiita, Y. Matsuda and A. Sasaki, *J. Crystal Growth*, 1984, **68**, 231.
2 A. Yoshikawa, S. Muto, S. Yamaga and H. Kasai, *J. Crystal Growth*, 1988, **86**, 279.
3 S. Yamaga, A. Yoshikawa and H. Kasai, *J. Crystal Growth*, 1988, **86**, 252.
4 A. C. Jones, *J. Crystal Growth*, 1994, **145**, 505.
5 P. J. Wright, B. Cockayne, A. J. Williams, A. C. Jones and E. D. Orrell, *J. Crystal Growth*, 1987, **84**, 552.
6 M. J. Almond, M. P. Beer, M. G. B. Drew and D. A. Rice, *J. Organomet. Chem.*, 1991, **421**, 129.
7 B. Cockayne, P. J. Wright, A. J. Armstrong, A. C. Jones and E. D. Orrell, *J. Crystal Growth*, 1988, **91**, 57.
8 A. C. Jones, *J. Phys. Paris II*, 1991, **C2**, 253.
9 K. F. Jensen, A. Annapragada, K. L. Ho, J.-S. Huh, S. Patnaik and S. Salim, *J. Phys. Paris II*, 1991, **C2**, 243.
10 P. J. Wright, P. J. Parbrook, B. Cockayne, A. C. Jones, E. D. Orrell, K. P. O'Donnell and B. Henderson, *J. Crystal Growth*, 1989, **94**, 441.

11 P. J. Wright, B. Cockayne, P. J. Parbrook, A. C. Jones, P. O'Brien and J. R. Walsh, *J. Crystal Growth*, 1990, **104**, 601.
12 M. J. Almond, M. P. Beer, K. Hagen, D. A. Rice and P. J. Wright, *J. Mater. Chem.*, 1991, **1**, 1065.
13 O. Briot, M. DiBlasio, T. Cloitre, N. Briot, P. Bigenwald, B. Gil, M. Averous, R. L. Aulombard, L. M. Smith, S. A. Rushworth and A. C. Jones, *Mater. Res. Soc. Symp. Proc.*, 1994, **340**, 515.
14 P. J. Wright, B. Cockayne, P. J. Parbrook, P. E. Oliver and A. C. Jones, *J. Crystal Growth*, 1991, **108**, 525.
15 M. A. Malik, M. Motevalli, J. R. Walsh, P. O'Brien and A. C. Jones, *J. Mater. Chem.*, 1995, **5**, 731.
16 O. F. Z. Khan, P. O'Brien, P. A. Hamilton, J. R. Walsh and A. C. Jones, *Chemtronics*, 1989, **4**, 244.
17 R. E. Linney and D. K. Russell, *J. Mater. Chem.,* 1993, **3**, 587.
18 H. Dumont, A. Marbeuf, J. Bouree and O. Gorochov, *J. Mater. Chem.,* 1992, **2**, 923.
19 H. Dumont, A. Marbeuf, J. Bouree and O. Gorochov, *J. Mater. Chem.,* 1993, **3**, 1075.
20 D. A. Jackson, *J. Crystal Growth*, 1989, **94**, 459.
21 H. Weller, *Angew. Chem., Int. Ed. Engl.*, 1993, **32**, 41.
22 H. Weller, *Adv. Mater.*, 1993, **5**, 88.
23 X. Li, J. R. Fryer and D. J. Cole-Hamilton, *J. Chem. Soc., Chem. Commun.*, 1994, 1715.
24 N. L. Pickett, D. F. Foster and D. J. Cole-Hamilton, *J. Mater. Chem.*, 1996, **6,** 507.
25 N. L. Pickett, D. F. Foster and D. J. Cole-Hamilton *J. Crystal Growth*, 1997, **170**, 476.
26 D. F. Foster and D. J. Cole-Hamilton, *Inorg. Synth.*, 1997, **31**, 29.
27 A. Rasencwaig, *Chemical analysis, Vol 57 Photoacoustics and Photoacoustic Spectroscopy*, Wiley, New York, 1980.
28 S. F. Bertram in *Handbook of X-Rays*, ed. E. F. Kaelble, McGraw-Hill, New York, 1967, pp 17–19.
29 S. W, Haggata, X. Li and D. J. Cole-Hamilton, *J. Mater. Chem.*, 1996, **6**, 1771.
30 A. Guinier, *X-Ray Diffraction*, W. H. Freeman, San Francisco, 1963, pp. 226–237.
31 R. B. Somoano, *Angew. Chem., Int. Ed. Engl.*, 1978, **17**, 238.
32 P. O'Brien and S. Haggata, *Adv. Mater. Opt. Electron.*, 1995, **5**, 117.
33 M. G. Bawendi, A. R. Kortan, M. L. Steigerwald and L. E. Brus, *J. Chem. Phys*, 1989, **91**, 7282.
34 A. Baronnet, *Rev. Mineral.*, 1992, **27**, 231.
35 N. N. Greenwood and A. Earnshaw, *Chemistry of the Elements*, Pergamon, Oxford 1974.
36 A. J. De Koning, J. Boersma and G. J. M. Van Der Kerk, *J, Organomet. Chem,* 1980, **195**, 1.
37 N. A. Bell and G. E. Coates, *J. Chem. Soc. A*, 1968, 823.
38 W. S. Rees, D. M. Green, T. J. Anderson, E. Bretschneider, B. Pathangey, C. Park and J. Kim, *J. Electron. Mater.*, 1992, **21**, 361.

Paper 7/01608E; *Received* 7*th March*, 1997